Data Analysis of Tracks of Heavy Ion Particles in Timepix Detector

S Hoang[1], R Vilalta[1], L Pinsky[2], M Kroupa[2], N Stoffle[2,3] and J Idarraga[2]

[1] Department of Computer Science, University of Houston, Houston, TX 77204, USA
[2] Department of Physics, University of Houston, Houston, TX 77204, USA
[3] Lockheed Martin, 1300 Hercules, Houston TX 77058, USA

E-mail: {smhoang, rvilalta, pinsky, mkroupa, nstoffle}@uh.edu, idarraga@cern.ch

Abstract. In this paper, we describe some of the computational challenges that need to be addressed when developing active Space Radiation Monitors and Dosimeters using the Timepix detectors developed by the Medipix2 Collaboration at CERN. Measurement of the Linear Energy Transfer (LET), the source and velocity of incident ionizing radiation, are of initial interest when developing such operational devices because they provide the capability to calculate the Dose-equivalent, and to characterize the radiation field for the design of radiation protective devices. In order to facilitate the LET measurement, we first propose a new method for calculating azimuth direction and polar angle of individual tracks of penetrating charged particles based on the pixel clusters they produce. We then describe an energy compensation method for heavy ion tracks suffering from saturation and plasma effects. Finally, we identify interactions within the detector that need to be excluded from the total effective Dose-Equivalent assessment. We make use of data taken at the HIMAC (Heavy Ion Medical Accelerator Center) facility in Chiba, Japan and NSRL (NASA Space Radiation Laboratory) at the Brookhaven National Laboratory in New York, USA for evaluation purposes.

1. Introduction

The rapid development in semiconductor detector technology at CERN has provided the capability to develop active personal dosimeters and radiation area monitors for use in space radiation environments [1]. The work reported here is based on the Timepix chip developed by the Medipix2 Collaboration at CERN, which when coupled with a Si sensor, can function as an active nuclear emulsion, allowing the visualization of the individual tracks created as the different incident particles traverse the detector [2]. The Timepix chip provides the capability of measuring the energy deposited by each incident particle that traverses the sensor layer. Together with the capability for online readout, this detector opens the door to a completely new generation of active Space Radiation Dosimeters and area monitors.

The Timepix chip is a CMOS-based pixel ASIC made of 256 x 256 pixels, each 55μm square, where the readout electronics for each pixel is embedded within the footprint of that pixel. The chip is attached to an overlying sensor layer using the Flip-Chip® bump-bonding technology. In this particular application, bulk n-type Si with p-type implants at each pixel interface is employed to enable the reverse biasing of the entire sensor layer, allowing the depletion of the free charge carriers from the sensitive volume to reduce noise. Pixel information is read-out in a frame that corresponds to

a 256 x 256 pixel image containing the digitized charge information collected during the acquisition time window. Based on the Timepix outputs, the measurement of Linear Energy Transfer (LET) [3], as well as the source and velocity of incident ionizing radiation [4][8], are attainable, and that information provides the capability to calculate the Dose-equivalent and to characterize the radiation field for future radiation protection purposes. The calculation of Dose-equivalent from the raw Absorbed Dose, which is simply the energy deposited per unit mass, requires the track-by-track multiplication of Absorbed Dose value by a Quality Factor that is a function of the LET of the particle producing the track. That Quality Factor can be as high as 30 for high LET tracks [5].

For a Timepix-based detector deployed in space, a penetrating energetic charged particle may be incident on the detector layer isotropically. While it is possible to determine the axis of the particle's trajectory through the sensor layer, there is an ambiguity in terms of the actual physical particle's direction of motion along that axis. By default, we assume that the particle direction is incident from above the sensor layer. There may be mechanisms, in some instances, to resolve the ambiguity, but we have not taken on that challenge yet. Calculation of the two angles --azimuth and polar angle-- described in Section 2 is a critical step in determining the LET, Dose-equivalent, charge and velocity of the particles.

Ionization along the primary particle track causes the creation of electrons and holes, which then drift under the influence of the applied bias voltage. As the carriers drift, they may interact with opposing sign charge carriers, which may result in recombination. This effect is enhanced at the highest densities of electrons and holes (the so-called "plasma-effect") [6]. The estimate of the amount of energy deposited based on the charge collected at the input to the Timepix is thus reduced when this occurs. This effect occurs to the greatest extent in the regions of highest ion density in the sensor, and when the bias voltage field direction is parallel to the track direction. Recombination may cause a reduced amount of energy in the measurement. However, the major losses are introduced by the non-linear response of the in-pixel front-end pre-amplifier stage and the effect of the front-end over-voltage protection diodes. These effects will clearly affect the uncertainty in LET calculations. A reconstruction technique described in Section 3 will be proposed to compensate for the energy loss due to these effects.

As the charged particles traverse the sensor, they may occasionally experience nuclear interactions within the sensor material. These interactions are normally rare and as such, negligible because of the small relative interaction cross section of the nucleus. However, because protons are by far the most common particles in the incident flux, the interactions of incident protons with detector material can produce short-range heavily ionizing nuclear fragments often enough, and these events can mimic genuine incident primary heavy ions that look like high LET particles. These misidentified heavy ions then in turn can contribute significant errors to the Dose-equivalent estimates due to their potentially large Quality Factors. Since our goal is the characterization of the incident radiation field, such interactions are of interest only insofar as we need to know what the primary incident particle was. Therefore, discrimination between these interactions and the tracks of genuine incident heavy ions need to be addressed in order to exclude them from the total effective Dose-Equivalent assessment. The interaction recognition will be shown in Section 4. Conclusion and future work will be described in Section 5.

2. Angle calculation method

When an event occurs, electrons and holes liberated along the particle's path drift in the electric field of the depletion bias voltage, diffusing both laterally and horizontally with respect to the field. The diffused charge will generally spread out over multiple pixels creating a cluster of pixels associated with a single event. This spreading follows a characteristic pattern such that the shape and energy intensity at pixels have precise information embedded within them about the azimuth direction and the angle of incidence with respect to the normal direction.

2.1. Azimuth direction determination

The shape of a cluster resembles a continent (using a geographic analogy) comprising a mountain in the center that is surrounded by peninsulas. Close study of the structure of clusters enabled us to identify three main components: a core part at the center of each cluster, the region immediately surrounding the core, that has been termed the "skirt", and an δ-ray part which comes from the higher energy recoil electrons liberated from the ionization process [3][8](Figure 1). The core contains most of the pixels with high energy, as it is the area where the detector collects most of the charges produced along the traversed path. The skirt contains lower energy pixels, where charge densities are low. The core and the skirt parts constitute the primary track, or continent. The δ-ray part can be considered as peninsulas connecting to the continent. The δ-ray part also contains low energy levels that provide estimates on the velocity or energy of the δ-rays embedded in their length and total energy. The δ-rays begin deep within the core and emerge through the skirt, where they can typically be distinguished clearly. The maximum possible δ-ray energy is a kinematic function of the velocity of the primary ion.

The core part can be used to calculate the azimuth direction, or slope of the track projected onto the plane of the detector. High-energy pixels provide more information about the direction than the low-energy pixels. Thus, instead of using a standard linear least squares fitting, we propose a weighted least square linear fit to find an equation of a line that best describes x-y data pairs of pixels in the core part. The energy at each pixel will be utilized as the weighing factor for this technique.

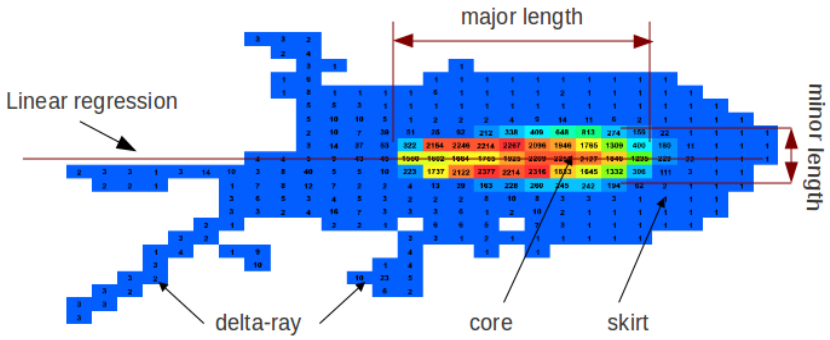

Figure 1. Cluster components

For computational reduction, we apply a threshold cut using a mean energy value of the cluster to get only pixels belonging to the core for model fitting. This threshold value will therefore exclude δ-ray and skirt pixels from data. In order to fit a line $y=\beta_0+\beta_1 x$ to pixels in the core of cluster, we minimized the function of weighted root mean square error as follows:

$$E = \sum e_i [y_i - (\beta_0 + \beta_1 x_i)]^2$$

where e_i is the energy of the pixel, β_0, β_1 are the intercept and the slope of the regression line. x_i, y_i are the coordinates of corresponding pixels in the detector coordinate. E is the error function. By solving this optimization problem, we can calculate the intercept and the slope of the regression line of the cluster as follows:

$$\beta_0 = \frac{\Sigma e_j x_j \cdot \Sigma x_i y_i e_i - \Sigma x^2{}_i e_i \cdot \Sigma e_j y_j}{\Sigma e_j x_j \cdot \Sigma e_i x_i - \Sigma x^2{}_i e_i \cdot \Sigma e_j} \qquad \beta_1 = \frac{\Sigma e_j y_j \cdot \Sigma x_i e_i - \Sigma x_i y_i e_i \cdot \Sigma e_j}{\Sigma e_j x_j \cdot \Sigma e_i x_i - \Sigma x^2{}_i e_i \cdot \Sigma e_j}$$

2.2. Polar angle calculation method

One of the biggest challenges in the determination of the uncertainty in the estimate of the polar angle is that the type of a charged particle at the point of penetrating Timepix chip is unknown. Each type

creates a distinct shape and energy on the projected plane of the detector. The δ-ray, skirt, and bias-voltage variation also affect the incident angle resolution. Also, the high-charge non-linearity effects need to be taken into account when they occur with the most heavily ionizing particles. We need to find a general pattern for all types of particles in order to come up with a method for accurately determining the angles of incidence.

We extract the effective *major* track length on the X-axis, and *minor* track width on the Y-axis as described in [3]. We then apply a new formula that combines the track length and width to obtain the best estimate of the angle. Note that using only the major length for angular estimation is not appropriate, as this length will vary considerably according to different applied bias-voltage and different unknown sources of particles.

$$\tan(\alpha) = \frac{D}{T}\left(major - \frac{minor}{2major - \text{minor}}minor\right)$$

In this equation, T=300 (μm) is the detector layer thickness, and D=55 (μm) is the distance between two pixels in the detector. The other constants are assigned by finding a reasonable fit to data for the angles and do not change as much for different configurations of the detector. Note that these assigned constants must satisfy the asymptotic principles in which *tan(α)* reaches ∞ as *major* reaches ∞ and *tan(α)*=0 as *major*=0. An additional requirement for the vertical track formulation is *tan(α)*=0 as *major=minor*. This formula ensures that the increasing or decreasing of both track lengths by bias-voltage variation effect does not have a big impact on the final angle resolution. Also, this formula can be applied for all types of heavy ion particles that are unknown at this point. D and T parameters can be changed according to a specific design of the Timepix chip and the associated sensor.

3. Energy compensation

3.1. Compensation method

The energy values are suppressed for the pixels in the middle of the clusters where the density of the charges and the resulting input voltages are very high (Figure 2). If we assume that a nominal cluster has the cone-shaped structure that was built by the more-or-less symmetrical accumulation of charges, the appearance of volcano would have to be filled in at a minimum. The slope of the exterior to the summit crater varies depending on the density of the charges. This summit crater needs to be compensated first by flattening out the top of cluster as shown in Figure 3. (Note that this step will not be necessary in the next generation of this technology, known as the Timepix 3 as it has a modified front end pre-amplifier design so that the cluster will have a flat top response for large charges and voltages at the input).

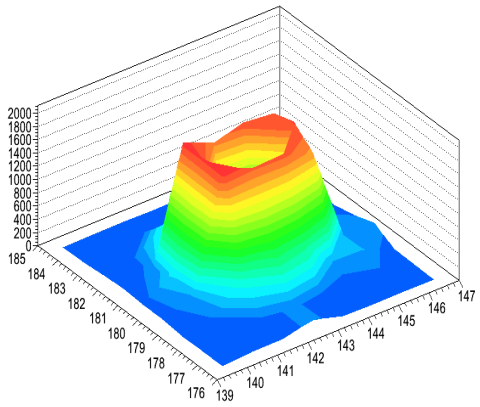

Figure 2. Volcano effect

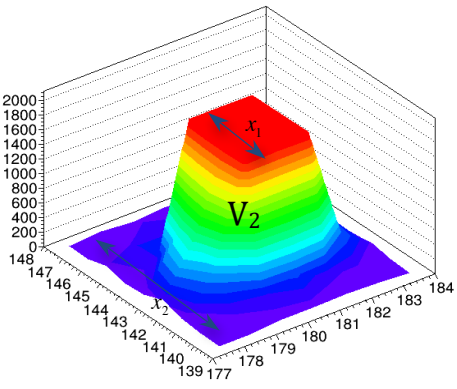

Figure 3. Energy compensation

We assume the total energy of the original cluster without suffering from volcano effect is V. After filling energy loss from the summit crater, we obtain total energy V_2. The remaining energy loss is the missing energy on the top of cluster, which is assumed as V_1. The purpose of the compensation process is to calculate V ($V=V_1+V_2$), given V_2 and the structure of cluster as in Figure 3. This structure allows calculations of minor projected track lengths x_1, x_2 at different the height of cluster according to different energy thresholds. We can calculate V in following equation.

$$V = V_1 + V_2$$

$$\frac{V_1}{V} = \frac{S_1 h_1}{S_2 h} = \frac{x_1 y_1 h_1}{x_2 y_2 h} = \left(\frac{x_1}{x_2}\right)^3$$

$$\frac{V - V_1}{V} = \frac{x_2^3 - x_1^3}{x_2^3}$$

$$\frac{V_2}{V} = \frac{x_2^3 - x_1^3}{x_2^3}$$

$$V = \frac{V_2 x_2^3}{x_2^3 - x_1^3}$$

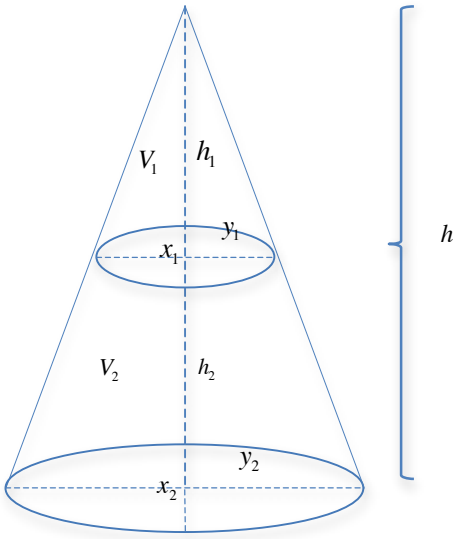

In the formula above, y_1, y_2 are major projected track lengths at different energy thresholds. h_1, h_2 are the height of V_1 and V_2, S_1 and S_2 are the projected area of V_1 and V_2 respectively. $h=h_1+h_2$ is the height of the original cluster after compensation. Note that these formulas are only valid with the assumption that a projected shape of cluster has ellipse-shaped or symmetric quadrilateral. In fact, experimental results show that the assumption is reasonable to yield compensated LET accurately to within 10% at most. A disadvantage of this compensation method is that it is very sensitive to the variation of applied bias voltage, which is affecting the diffusion of charges and cluster structure.

3.2. Incident angle and energy compensation evaluation

We perform an analysis to determine incident angle, LET values for the tracks and evaluate the compensation method. Table 1 shows the LET estimation using angular resolutions described above, combined with total energy deposited from energy calibration method as described in [3]. The LETs generated from different angles are expected to be the same because the relatively small thickness of the sensor does not typically induce a significant variation in heavy ion LET (due to the reduction in the kinetic energy of the incident particle). In this table, the calculated LET values of the particles from H (50, 100MeV), He (100, 180MeV), C (300MeV), O (430MeV), N (290MeV) are very close to the ones calculated from SRIM simulation even for different angles. The high charge non-linear effects do not occur with these particles.

Due to the high charge non-linear effects, which may come in part from the recombination of high densities of electrons and holes, the estimate of the amount of energy deposited is reduced for particles at the end of the table (Si-400MeV, Ar-290MeV, Fe-400MeV), although the angles are well estimated. The red numbers in this table represent raw calculated LET values without compensation for the non-linear effects. The black numbers of the same cell show results after making a correction using the method described in Section 3.1. The corrected mean values of these are close to what is expected. The RMS representing the spread of statistical LET distribution is still big due to the saturation effect. As noted above, the new version Timepix 3 will solve this problem by removing the saturation effect and by providing a flat response region on the top of the volcano.

Table 1. Angle and LET resolution

	SRIM	0 degree		30 degree		60 degree		75 degree	
	Kev/um	Angle	LET	Angle	LET	Angle	LET	Angle	LET
H-50	**2.3**	**8.4**±6.9	**2.26**±0.27	**28**±3.5	**2.27**±0.28	**59.7**±1.7	**2.27**±0.25	**74.2**±1.56	**2.35**±0.24
H-100	**1.36**	**0.6**±1.3	**1.4**±0.3	**30.2**±3.8	**1.3**±0.3	**59.7**±1.2	**1.26**±0.3	**74.5**±1.3	**1.3**±0.3
He-100	**5.42**	**2.1**±6.8	**5.5**±0.75	**30.2**±3.7	**5.67**±0.54	**60.1**±1.3	**5.7**±0.6	**74.7**±1.5	**6.0**±0.54
He-180	**3.65**	**4.7**±7.2	**3.65**±0.5	**29.3**±3.5	**3.8**±0.6	**60.3**±1.4	**3.7**±0.5	**74.6**±1.04	**3.76**±0.4
C-300	**23.0**			**29.7**±4.3	**25.4**±3.6	**60.9**±3.6	**26.6**±4.1		
C-400	**20.0**	**2.1**±5.2	**20.01**±2.8			**60.4**±1.2	**20.6**±2.2		
O-430	**35.0**	**4.3**±6.2	**32.2**±7.7	**29.7**±3.6	**38.8**±5.4	**60.1**±1.3	**39.6**±4.8	**74.7**±0.6	**41**±4.4
N-290	**32.0**	**4.3**±6.6	**31.0**±7.6	**29.1**±3.6	**29.1**±2.8	**60.5**±1.1	**31.9**±2.7	**75.2**±0.6	**33**±2.8
Si-400	**110.0**	**2.6**±3.5	**106.0**±18.8 **57.2**±5.1	**25.5**±4.6	**113**±24.2 **65.5**±6.1	**59.5**±1.8	**125**±17.0 **74.9**±4.9		
Ar-290	**225**	**4.9**±7.6	**219.2**±18.9 **88.15**±8.3	**20**±6.4	**237**±19.5 **97.6**±6.6	**59**±1.57	**218.5**±15.8 **102**±5.98		
Fe-400	**377.0**	**3.8**±4.5	**374.0**±40.4 **126.3**±8.2	**24.1**±5.2	**380**±49.0 **137**±9.5	**61.6**±1.1	**328**±40.5 **134.7**±12.1	**75.9**±1.5	**340**±23.8 **141.8**±11.2

4. Interaction recognition

In order to identify the variety of patterns of clusters created from interactions, we conducted experiments with a large sample of proton energies. From that data we can separate high LET clusters that are definitely products of proton interactions. We have been able to identify different types of interactions associated with following patterns:

- **Interaction with two of more clear peaks.** A proton interacts with a Si nucleus producing two or more heavy ions connecting via lower energy pixels. This pattern can be easily recognized by using a suitable energy threshold cut and calculating number of connecting components from the remaining pixels.

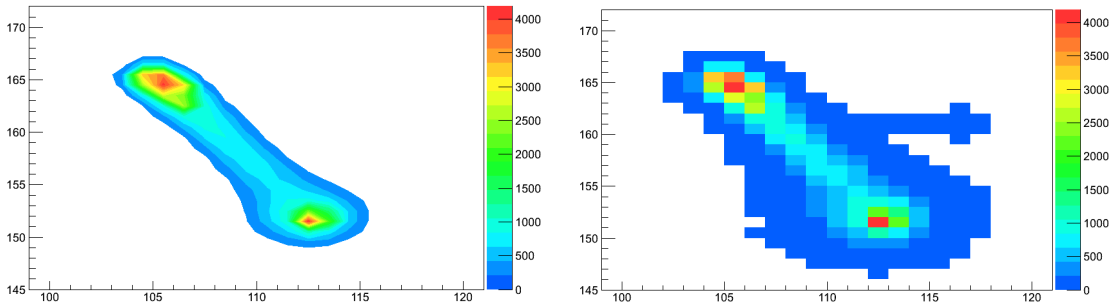

Figure 4. Interaction with 2 primary fragments

- **Interaction that creates a stopping particle**: This interaction transmutes the Si nucleus into a slow particle that ranges immediately or shortly at the vicinity of interaction position. As a result, the forming cluster contains characteristics similar to products of captured neutron with round shape, special morphology, or stopping particle with Bragg curve structure.

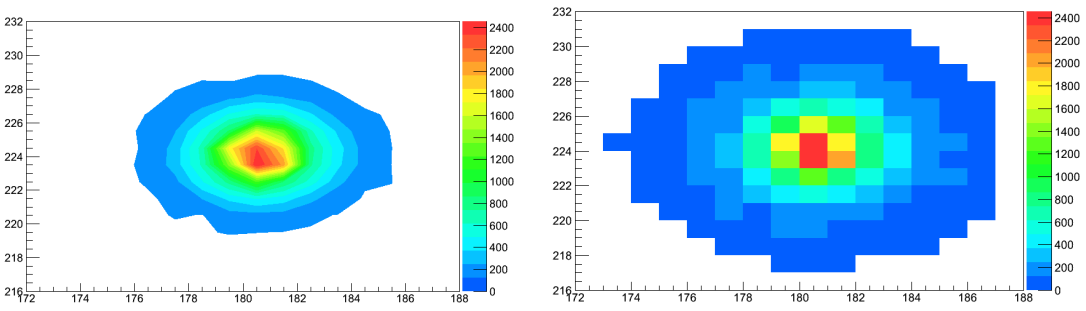

Figure 5. Interaction with stopping

- **Interaction with visible fragments surrounding primary particle**: Unlike the first case, which produces two or more primary fragments, this interaction creates one primary core of cluster and secondary fragments that are clearly different from the skirt of a genuine cluster. We use distance transform [7] to determine levels of pixels and the core of the primary. Calculating the average distance between pixels level 3 in the core and remaining pixels level 2 will help to recognize pixels of fragments. In a genuine cluster, pixels of levels 2 must be the immediate neighbors of pixels level 3 in the core, but this is not the case for these interacting clusters.

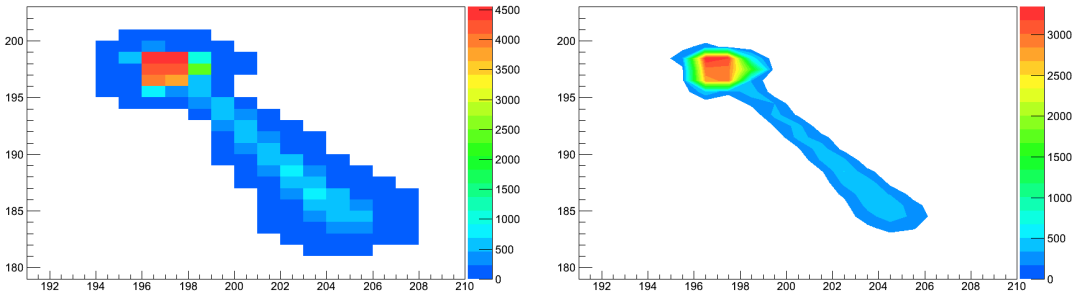

Figure 6. Interaction with one primary and one surrounding secondary

- **Interaction with fragments similar to delta rays**: Similar to the third case, the cluster consists of one primary fragment surrounded by many other fragments. However, the surrounded fragments that mimic the δ-rays are not easy to recognize. We also use the distance transform to isolate the core and calculate the number of inner pixels in fragments. The number of inner pixels will help us determine whether secondary particles are δ-rays or interaction fragments.

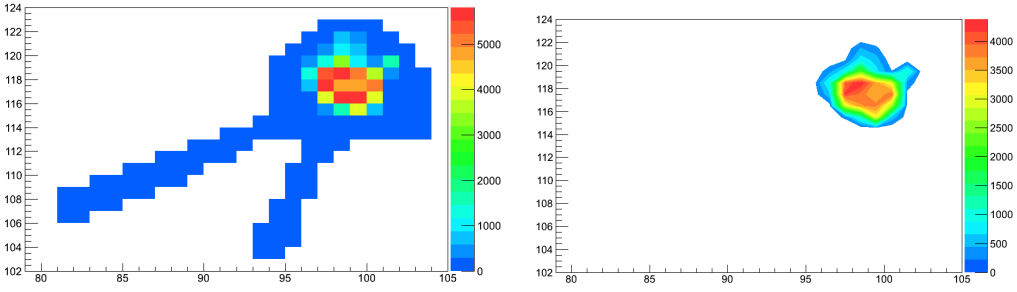

Figure 7. Interaction with one primary and fragments similar to delta-ray

5. Conclusion and future work

In this paper, we proposed a new method for calculating azimuth direction and polar angle of individual tracks of penetrating charged particles, which is a critical step to estimate LET and Dose-equivalent. We then described an energy compensation method to make a correction of LET for heavy ion tracks suffering from plasma effects. Finally, we identified interactions to exclude them from the total effective Dose-Equivalent assessment. Future work will focus on data analysis of delta-rays, which reflect the energy of primary particles, and extract relevant features for identification of ion charge and velocity.

Acknowledgments

The authors would like to express thanks the contributions of the Medipix2 collaboration, HIMAC, and the financial support of NASA Johnson Space Center. We would like to thank the following people in particular: A. Empl, S. Pospisil, Z. Vykydal, D. Turecek, E. Semones, K. Lee, N. Zapp, A. Bahadori, H. Kitamura, N. Yasuda, and Y. Uchihori for their substantial contribution to this research project.

References

[1] Pinsky L, Empl A, Hoang S, Stoffle N, Jakubek J, Vykydal Z, Turecek D, Pospisil S, Kitamura H, Ploc O, Uchihori Y, Yasuda N, Amberboy C, Hauss J, Lee K, Semones E, Zapp N, Parker R and Cooke D 2012 Preparing for the First Medipix Detectors in Space. *Pro. of the IEEE Aerospace Conf.*, Big Sky, Montana

[2] Llopart A, Ballabriga R, Campbell M, Tlustos L and Wong W 2007 Timepix, a 65k programmable pixel readout chip for arrival time, energy and/or photon counting measurements. *Nucl. Inst. And Meth. Phys. Res.*, A **581**, 485-494

[3**]** Hoang S, Pinsky L and Vilalta R 2012. LET Estimation for Heavy Ion Particles based on a Timepix-based Si Detector. *Int. Conf. on Comp. in High Energy and Nucl. Phys. (CHEP-12)*, New York, USA

[4] Pinsky L, Empl A, Gutierrez A, Jakubek J, Kitamura H, Miller J, Leroy C, Stoffle N, Pospisil S, Uchihori Y, Yasuda N and Zeitlin C 2011 Penetrating heavy ion charge and velocity discrimination with a TimePix-based Si detector (for space radiation applications). *Nucl. Instr. and Meth.* A **633** 190-193

[5] National Council on Radiation Protection 2003 Information Needed to Make Radiation Protection Recommendations for Space Missions Beyond Low-Earth Orbit, *NCRP Report No. 153*

[6] Williams R and Lawson E 1974 The plasma effect in silicon semiconductor radiation detectors. *Nucl. Instr. and Meth.* **120** 261-268

[7] Fabbri R, Costa L, Torelli J and Bruno O 2008 2D Euclidean distance transform algorithms: A comparative survey. *ACM Comp. Survey* **40**

[8] Stoffle N, Pinsky L, Hoang S, Idarraga J, Kroupa M, Jakubek J, Turecek D and Pospisil S 2009 Initial results on charge and velocity discrimination for heavy ions using silicon-Timepix detectors, *JINST 7* C **1**